Check for updates
physica status solidi rrl
www.pss-rapid.com

# Experimental Verification of Single-Type Electron Population in Indium Tin Oxide Layers

*Sebastian Złotnik,* Alessandro Pianelli, Jacek Boguski, Marek A. Kojdecki, Paweł Moszczyński, Janusz Parka, and Jarosław Wróbel*

**Accurate determination of electronic transport properties of individual transparent conductive oxide layers, namely indium tin oxide (ITO), is essential for further development and design of photonic devices with ITO layer as a tunable ultrafast optoelectronic component. Precise magnetotransport measurements are here implemented to achieve carrier mobility distribution that gives insight into types and characteristics of carrier species. ITO thin films with various sheet resistance of ≈10, 75, and 350 $\Omega$ sq$^{-1}$, respectively, are examined at near-room temperature. Unimodal mobility distribution is revealed in ITO films, independently on their resistivity, with no evidence of unseparated contributions from surface or interface states. The electron mobility varies depending on ITO's resistivity, ranging from 36.8 to 47.2 cm$^2$ V$^{-1}$ s$^{-1}$ at 300 K. Importantly, no minority hole conduction is present. The ITO thin films exhibit solely bulk-like conduction with an absence of parallel conductions. In addition, the existence of single-type electron population in ITO that can be viewed as an important validation of exclusively donor-type defects and/or impurities contributing to total ITO conductivity is experimentally confirmed. These results indicate that ITO can be viewed as an integrated counterpart for photonic metadevices.**

## 1. Introduction

Full understanding and control of the charge carriers in nanophotonic devices are not yet entirely achieved. In fact, it is one of the foremost challenges that photonic community deals with. For instance, superconductivity and ultrafast electro-optical switching materials are of particular interest nowadays in photonic architectures.[1] One of the long-lasting goals in electro-optical devices is to speed up data rate and reduce energy consumption. This is mainly due to an increasing demand of the acquisition/processing data rate. In this view, nonlinear devices are one of the most eligible platforms that eventually meets criteria like[2] 1) interplay of low power and intense response, 2) femtosecond time response, and 3) complementary metal-oxide-semiconductor (CMOS)-compatible technology.

Since the middle of the last century, a deep investigation of semiconductor compounds has led to unprecedented technological innovations.[3] Despite that, conventional semiconductors partially meet the aforementioned criteria, though several drawbacks still limit the use of them in the next generation of high-speed technology.[4] A class of materials that reveal an vast potential in this field is related to certain transparent conductors, mainly oxides. These materials have been intensively developed due to rapid growing markets, such as display technologies, a novel concept of photovoltaic systems, and solid-state lightning, just to name a few.[5] Materials referred as transparent conductive oxides (TCOs),[6] such as doped ZnO, $In_2O_3$, and $SnO_2$, play important roles, but other compounds with perovskite structures, for example, vanadites ($SrVO_3$ and $CaVO_3$), were demonstrated to be attractive candidates to enhance electro-optical performances.[5a] In particular, a ternary compound, indium tin oxide (ITO), has become a widely used TCO in the optics and industry sector, mainly due to its figure of merit:[7] optical transparency and electrical conductivity.

Yet, ITO has been demonstrated to possess peculiar electro-optical properties in its crossover frequency when the dielectric permittivity changes sign from positive to negative, a singular optical regime often called epsilon-near-zero (ENZ). In its ENZ regime, it is possible to observe large optical nonlinearities and ultrafast response,[8] thus leading to consider ITO as a CMOS-compatible platform for ultra-fast nanophotonics.[9] Recently, ITO was also

S. Złotnik, A. Pianelli, J. Boguski, J. Parka, J. Wróbel
Institute of Applied Physics
Military University of Technology
2 Kaliskiego Street, 00-908 Warsaw, Poland
E-mail: sebastian.zlotnik@wat.edu.pl

A. Pianelli
Faculty of Engineering and Natural Science, Photonics
Tampere University
Tampere 33720, Finland

M. A. Kojdecki
Institute of Mathematics and Cryptology
Military University of Technology
2 Kaliskiego Street, 00-908 Warsaw, Poland

P. Moszczyński
Institute of Computer and Information Systems
Military University of Technology
2 Kaliskiego Street, 00-908 Warsaw, Poland

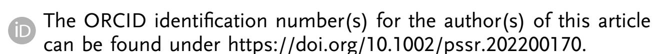
The ORCID identification number(s) for the author(s) of this article can be found under https://doi.org/10.1002/pssr.202200170.

© 2022 The Authors. physica status solidi (RRL) Rapid Research Letters published by Wiley-VCH GmbH. This is an open access article under the terms of the Creative Commons Attribution-NonCommercial-NoDerivs License, which permits use and distribution in any medium, provided the original work is properly cited, the use is non-commercial and no modifications or adaptations are made.

**DOI: 10.1002/pssr.202200170**

demonstrated to be an effective broadband metasurface layer,[10] platform for biosensing,[11] as a metatronic board in analog computing [12] or fast gigahertz Mach–Zehnder modulator.[13]

ITO, in fact referred to also as Sn-doped $In_2O_3$, is a well-known n-type degenerate semiconductor with a wide bandgap ranging between 3.5 and 4.3 eV. Alternatively, ITO is considered as a low-carrier-concentration and disordered conductor, suggesting that it is rich in quantum-interference transport phenomena.[14] Generally, it is recognized that defects and impurities lead to high unintentional carrier densities present in TCOs.[15] Moreover, besides impurities such as hydrogen and several native defects, it is believed that also surface and interface states contribute to total conductivity of some TCOs, mainly with a donor-like nature.[16] The relevant electronic parameters of ITO were frequently investigated, primarily by conventional Hall effect measurements. Nevertheless, the origins of conductivity in ITO are still not fully understood and more experimental evidence is needed.

Though ITO has been proven to be an optimal material in optoelectronic devices for visible region of the electromagnetic spectrum, a thorough investigation of carrier mobility distribution has not been well addressed. Indeed, to consider ITO as a potential candidate for further development of the next generation of optoelectronic components, precise determination of charge carrier transport properties is worth to be established. Therefore, in this work, we present conductivity analyses of three ITO films with different thicknesses: 185, 23, and 20 nm, and with nominal sheet resistance ($R_{sh}$) of 10, 75, and 350 Ω $sq^{-1}$, respectively. The ITO films were selected intentionally due to their substantial difference in sheet carrier concentration, changing within nearly two orders of magnitude, representing the most common commercially available ITOs. The studies were performed by applying magnetic field-dependent Hall effect and resistivity measurements, assisted with mobility spectrum analysis (MSA). It was revealed that indeed a unimodal mobility distribution with pure electron conduction can be detected. We demonstrate the existence of a single-type electron population in all the ITO films with no evidence of unseparated contributions from surface or interface states, either at 273 or 300 K. The obtained data may give an insight for potential circuitry technology based on single-electron/photon channels for data storage devices integrated with ITO as a board customization.

## 2. Results and Discussion

Temperature-dependent Hall effect and resistivity measurements at constant magnetic field, $B = 0.54$ T, were initially performed to obtain $R_{sh}$, as well as the Hall carrier concentration ($n_{Hall}$) and averaged Hall mobility ($\mu_{Hall}$); see **Figure 1**. These particular characterizations are normally conducted for electronic devices, usually at various temperatures. Importantly, the electrical contacts were comprehensively characterized in order to obtain reliable Hall effect datasets; see the description in Section 1 in the Supporting Information (SI). $R_{sh}$ derived from Hall effect measurements is plotted in Figure 1a. This parameter can be conveniently determined by implementing van der Pauw resistivity measurement technique.[17] The derived $R_{sh}$, ≈10, 75 and 350 Ω $sq^{-1}$, agrees well with nominal values provided by the supplier. $R_{sh}$ values were recorded at 300 K. The $R_{sh}$ of ITO is strongly thickness dependent, the greater the thickness, the lower the resulting $R_{sh}$; this trend was already observed in ITO.[18] Taking into account nanometric thickness of the studied ITO films, resistivity ($\rho$) that is $\approx 10^{-4}$ Ω cm can be estimated. Li and Lin presented $\rho$ for two ITO films with various thicknesses (125 and 240 nm), ranging at room temperature from 1.89 to $2.63 \times 10^{-4}$ Ω cm.[19] Generally, the $\rho$ of ITO was reported to decrease by only around 10% in the temperature range of 300–100 K,[19,20] displaying classical metallic behavior. Importantly, $\rho$ and $n_{Hall}$ of ITO are strongly dependent on deposition processes and conditions,[21] meaning that the industrial

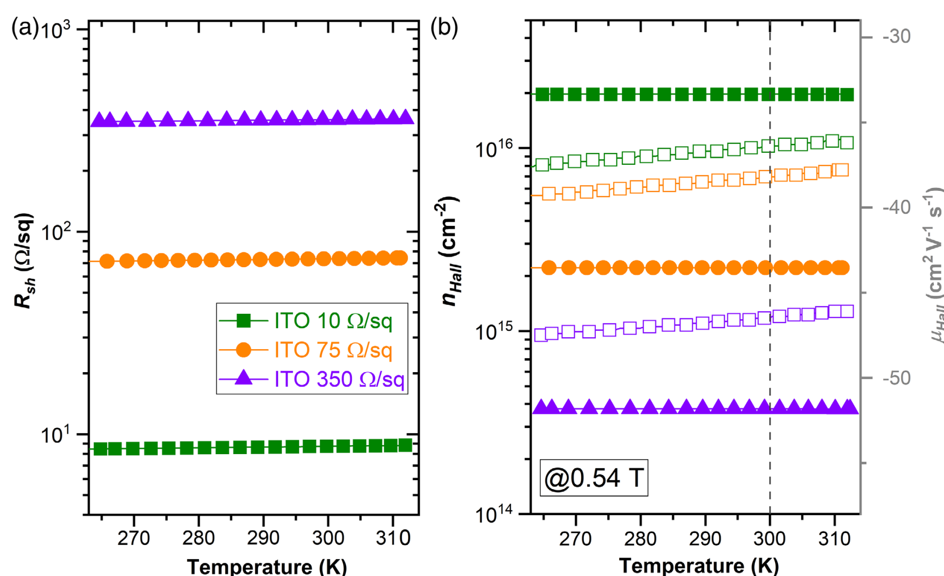


**Figure 1.** Hall effect measurement results derived at single $B$ equal to 0.54 T, showing temperature dependence of a) $R_{sh}$ and b) $n_{Hall}$ (closed symbols) and $\mu_{Hall}$ (open symbols) of all ITO films. Room temperature (300 K) is marked in graphs by dashed lines.


© 2022 The Authors. physica status solidi (RRL) Rapid Research Letters published by Wiley-VCH GmbH

production method determines its electro-optical parameters. More electrical datasets can be found in a topical review dedicated to electronic conduction properties of ITO.[14]

The commonly determined carrier characteristics, $n_{Hall}$ and $\mu_{Hall}$, in the temperature range of 265–315 K, are depicted in Figure 1b. The ITO structures show a rather constant temperature trend of $n_{Hall}$ and $\mu_{Hall}$, and the Hall measurements data reveal that transport is governed by electrons. The $n_{Hall}$ values are in good agreement with reported ones,[21,22] being at 300 K $\approx 2.0 \times 10^{16}$, $2.2 \times 10^{15}$, and $3.8 \times 10^{14}$ cm$^{-2}$ for ITO 10, ITO 75, and ITO 350 Ω sq$^{-1}$, respectively. Regarding $\mu_{Hall}$, it ranges from 36 to 46 cm$^2$ V$^{-1}$ s$^{-1}$ at 300 K. Interestingly, Koida and co-workers explored amorphous and crystalline $In_2O_3$-based films (including Sn doped),[23] demonstrating that polycrystalline $In_2O_3$:Ce,H films can exhibit $\mu_{Hall}$ greater than 100 cm$^2$ V$^{-1}$ s$^{-1}$ at room temperature.

Furthermore, a core analysis in the present work, magnetic-field-dependent Hall effect measurement, was carried out in order to evaluate potentially multiple carrier types present in ITO films. In such magnetotransport measurements, the changes in the conductivity (or resistivity) tensors of materials caused by an application of magnetic field can be traced. Importantly, the measurements data were intentionally conducted at near-room temperatures (at 273 and 300 K), avoiding possible quantum effects, such as Shubnikov–de Haas oscillations, that often dominate in electronic transport processes at high *B*, low temperatures, and/or in ultrathin films. Therefore, longitudinal and transverse conductivity tensor components in the in plane ($\sigma_{xx}$ and $\sigma_{xy}$) were derived from the experimental Hall effect and resistivity data and are plotted as a function of *B* in **Figure 2**a (*B* in log scale); relations to Hall effect data can be found in the study by Wrobel et al.,[24] while the scheme showing Hall effect measurements with particular indications of axis (coordinate system) is depicted in Figure 2b. Here, the $\sigma_{xx}$ and $\sigma_{xy}$ demonstrate quite similar tendency, independently on $R_{sh}$ of ITO films; for low *B*, $\sigma_{xx}$ tends to the highest values while $\sigma_{xy}$ goes from zero toward negative values as *B* increases. Behavior of $\sigma_{xy}$, with a negative sign over the entire *B* range, indicates a dominance of electrons. The accurate determination of the conductivity components is crucial for the resulting MSA to be valid.

The mobility spectra, $S(\mu)$, are obtained from the *B* dependence of conductivity tensor components: $\sigma_{xx}(H)$ and $\sigma_{xy}(H)$. The methodology of MSA implementation is described in our previous works.[24,25] MSA was proven to be effective approach toward precise determination of parallel conductions in various compounds, such as oxides,[26] arsenides,[24] nitrides,[27] or topological materials.[28] Figure 2c illustrates calculated mobility spectra, $S(\mu) \geq 0$, of ITO films with different $R_{sh}$, derived at 300 K; see the Section 2 of the SI for calculated $S(\mu)$ at 273 K. Clearly, a single-type electron population can be revealed in ITO films with no evidence of unseparated contributions from surface or interface states, at least in the near-room temperature range; furthermore, no minority hole conduction is present. In fact, bulk-like conduction is solely present in the studied ITO thin films (no indication of parallel conductions). In addition, an estimated electron concentration, $n_e$, was found to be $\approx 1.99 \times 10^{16}$, $2.21 \times 10^{15}$, and $3.76 \times 10^{14}$ cm$^{-2}$ for ITO 10, ITO 75, and ITO 350 Ω sq$^{-1}$, respectively, thus, $n_e$ is in very good agreement with $n_{Hall}$. Importantly, electron accumulation was identified at the surface of undoped $In_2O_3$ films, but it was proven that in heavily Sn-doped $In_2O_3$, an electron depletion layer does not exist at the surface due to moving a charge neutrality level.[16d] In other conventional semiconductors, nominally undoped In-containing binary compounds, namely InAs and InN,[29] downward band bending was found to be extreme, resulting in the observed large accumulation of electrons at the surface. In this context, our experimental results can be viewed as an important verification, not obvious to an entire community familiar with these compounds.

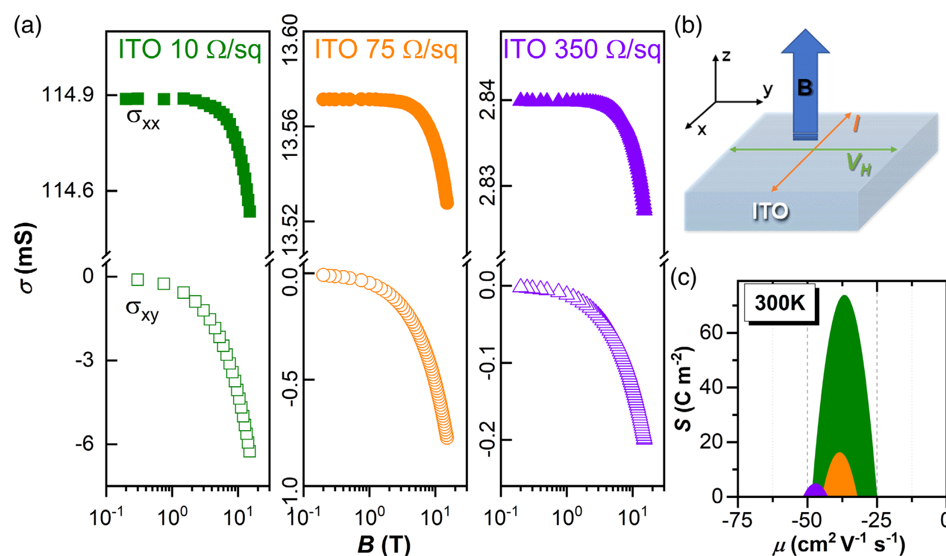


**Figure 2.** a) The conductivity tensor components $\sigma_{xx}$ (closed symbols) and $\sigma_{xy}$ (open symbols) as a function of *B* at 300 K. b) Scheme presenting Hall effect measurements: *B*, Hall voltage ($V_H$), and current (*I*) is included with coordinate system as an inset. c) $S(\mu)$ derived at 300 K from fitting $\sigma_{xx}$ and $\sigma_{xy}$, resulting in single-type electron channel conductivity in ITOs.


© 2022 The Authors. physica status solidi (RRL) Rapid Research Letters published by Wiley-VCH GmbH

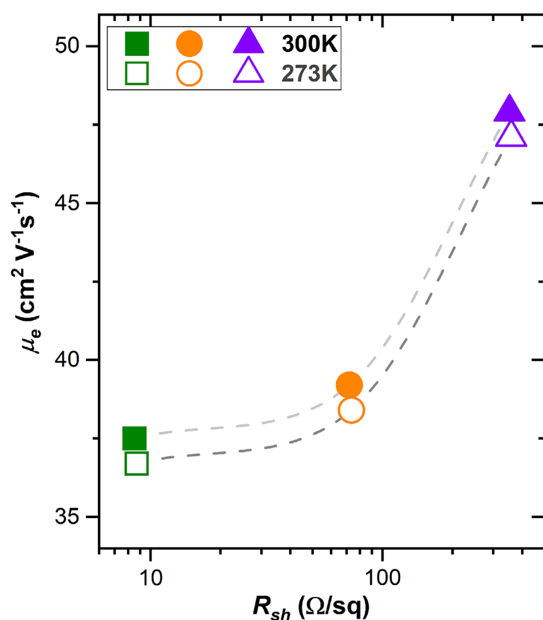


**Figure 3.** Mean $\mu_e$ as a function of $R_{sh}$ (in a log scale) derived from $S(\mu)$ at 273 and 300 K; dashed lines are used as a guide for the eye.

The most relevant findings derived from S(μ) are collected in **Figure 3**, showing dependence of mean electron mobility, $\mu_e$, as a function of $R_{sh}$ at 273 and 300 K. The mean $\mu_e$ (pure electron population) varies depending on sample's $R_{sh}$ and temperature, being 36.8, 38.4, 47.2 cm$^2$ V$^{-1}$ s$^{-1}$ at 300 K and 37.6, 39.2, 48.0 cm$^2$ V$^{-1}$ s$^{-1}$ at 273 K, for ITO 10, ITO 75, and ITO 350 Ω sq$^{-1}$, respectively. The acquired $\mu_e$ values are very similar to $\mu_{Hall}$. This definitely proves that reported elsewhere effects, such as an interface-induced disorder present in degenerate semiconductor films on semi-insulating substrates,[22c,30] or surface states, either with a donor- or an acceptor-like character,[15a] can be excluded. Our studies do not detect any of aforementioned effects, showing that there is an absence of low-mobility interface or surface electron accumulation layers, in particular analyzed here ITO with bulk carrier concentration higher than 10$^{20}$ cm$^{-3}$. In other scenarios, a modification of electron mobility distribution due to a change in scattering behavior upon charging might be also a possible reason. However, such effect was observed but in ultrathin films, up to 10 nm thick.[31] There is also a visible parallel shift in $\mu_e$ between two selected temperatures. It is an evidence of a certain scattering mechanism, being a subject of debate for decades in ITO. The mechanisms limiting $\mu_{Hall}$ in ITO were already demonstrated in several works.[32] Kikuchi and co-workers revealed that the $\mu_{Hall}$ of nontreated ITO exhibited a negative temperature dependence at temperatures above 150 K, indicating phonon scattering to be a dominant mechanism.[32c] Valla et al. stated that a predominant mechanism governing $\mu_{Hall}$ (for $n_{Hall}$ in a range of 10$^{20}$–10$^{21}$ cm$^{-3}$) is either associated with scattering at neutral or ionized impurities.[32f] The very recent work of Sharika and co-workers emphasized on the other hand that the microstructural features strongly affect electron mobility.[32g] However, more comprehensive experimental MSA data collection on ITO films with different crystallinity, carrier concentration, and $S(\mu)$ derived at various temperatures should be carried out to speculate which scattering mechanism is more prominent. It is actually a subject of our further studies.

## 3. Conclusion

In summary, we experimentally validate a unimodal mobility distribution present in the considered ITO films via magnetotransport measurements assisted with MSA conducted at near-room temperatures. We show that the high conductivity of ITO films is solely due to electron carriers to which no hole contributions have been identified. The mean $\mu_e$ varies depending on sample's $R_{sh}$ and temperature, being 36.8, 38.4, and 47.2 cm$^2$ V$^{-1}$ s$^{-1}$ at 300 K for ITO 10, ITO 75, and ITO 350 Ω sq$^{-1}$, respectively. Particularly, the acquired $\mu_e$ values are very similar to conventionally derived $\mu_{Hall}$, proving an absence of low-mobility interface or surface electron accumulation layers. Considering that the technological perspectives go toward new electro-optical components with a good tradeoff between low power consumption united to high transparency and good conductivity, ITO emerges as a prominent candidate for metadevice components in applications like electromagnetic interference (EMI) shielding, transparent antennas, and solar cells. In addition, the single-type electron population presented in ITO can be seen as an opto-electronic peculiarity in the design of transparent electronic device schemes with singular functionalities.

## 4. Experimental Section

*ITO Thin Films*: Commercially available ITO films (three specimens), acquired from Guangzhou Lepond Glass Co., Ltd (China) and mainly used in electro-optical devices and microelectronics, were devoted for magnetotransport characterization. ITOs were deposited on a float glass substrate (either 0.7- or 1.1 mm-thick plates), with a nominal thickness of 185 ± 20, 23 ± 5, and 20 ± 5 nm with $R_{sh}$ of ≈10, 75, and 350 Ω sq$^{-1}$, respectively.

*Structure Processing*: The Hall effect measurements were carried out on the symmetrical square samples in van der Pauw geometry. The ITO films were fully processed by including positive photolithography to define samples with dimensions of 4 × 4 mm. The following steps were included: 1) surface washing with acetone to eliminate particulates, 2) spin coating (2500 rpm for 1 min) of photoresist (AZ 4533) to obtain a homogeneous layer (≈3 μm thick), 3) a photoresist hardening on a hot plate (115 °C for 2 min), 4) UV lightning with a dose of 120 mJ cm$^{-2}$ through a chrome glass mask, and 5) sample treatment using 0.2 M NaOH aqueous solution for 100 s. Such lithographically processed ITO films were then cut along straight lines by an automatic dicing saw DAD3220 (Disco Corp., Japan). Indium granules with a purity of 99.995% were used to make the electrical contacts. Due to the good wettability of the ITO surface by In, it was possible to obtain symmetrical contacts with high adhesion to oxide surface. The as-processed ITO 10, ITO 75, and ITO 350 Ω sq$^{-1}$ structures were mounted on the 6-pin sample platform with a small amount of Araldite two-component epoxy adhesive. The contact pads were connected to the pins of the sample platforms by soldering Au wires with a diameter of 25 μm.

*Electrical and Magnetotransport Characterization*: The core characterization was conducted using a superconducting 16T cryogen-free magnet system (CFMS) equipped with cryostat, fabricated by Cryogenic Ltd. The samples fixed to holders and located on a variable temperature insert were directly placed in the circulating high-purity He gas (coolant agent) at a constant pressure (closed-cycle mode). Such conditions ensure relatively good temperature stabilization (≲50 mK), monitored by Cernox sensor.


© 2022 The Authors. physica status solidi (RRL) Rapid Research Letters published by Wiley-VCH GmbH

The Hall effect measurements were performed in the temperature range of 260–315 K (ramp rate of 0.5 K $min^{-1}$) at a constant *B* of 0.54T as well as at variable *B* up to 15T (at 273 and 300 K), perpendicular to the ITO surface. The Hall effect sample structure was placed in the center of the ±16T electromagnet solenoid, where the *B* homogeneity was greater than ≤0.1% with total variation over a 10 mm-diameter sphere. The van der Pauw test structures were electrically pre-examined in the temperature range of 260–315 K on cooling to assess the symmetry and linearity of current–voltage (*I*–*V*) characteristics of all contact pairs and to select appropriate bias conditions for the resistivity and Hall effect measurements.

## Supporting Information

Supporting Information is available from the Wiley Online Library or from the author.

## Acknowledgements

This research was primarily conducted with the financial support under the program of the Minister of Science and Higher Education (Poland): "Regional Excellence Initiative" in 2019–2022; project number 014/RID/14 2018/19, funding amount of PLN 4 589 200.00 (rid.wtc.wat.edu.pl). A.P. individually acknowledges the Polish National Agency for Academic Exchange (NAWA), and the Instituto Polacco di Roma in the framework of exchange programme for students and scientists as part of bilateral cooperation Italy-Poland 2021–2022 granted by no. BPN/FRC/2021/1/00008/U/01. A.P. also acknowledges the European Social under the "Operational Programme knowledge Education Development 2014–2020".

## Conflict of Interest

The authors declare no conflict of interest.

## Data Availability Statement

The data that support the findings of this study are available from the corresponding author upon reasonable request.

## Keywords

electron conduction, Hall effects, indium tin oxide, mobility spectra, transparent conductors

Received: May 4, 2022
Revised: June 9, 2022
Published online: July 5, 2022

[1] a) R. Dhama, A. Panahpour, T. Pihlava, D. Ghindani, H. Caglayan, arXiv **2021**; b) V. Caligiuri, A. Pianelli, M. Miscuglio, A. Patra, N. Maccaferri, R. Caputo, A. De Luca, *ACS Appl. Nano Mater.* **2020**, *3*, 12218; c) V. N. Smolyaninova, C. Jensen, W. Zimmerman, J. C. Prestigiacomo, M. S. Osofsky, H. Kim, N. Bassim, Z. Xing, M. M. Qazilbash, I. I. Smolyaninov, *Sci. Rep.* **2016**, *6*, 34140.

[2] a) Y. Zhao, Y. Yang, H.-B. Sun, *PhotoniX* **2021**, *2*, 3; b) T. Volz, A. Reinhard, M. Winger, A. Badolato, K. J. Hennessy, E. L. Hu, A. Imamoğlu, *Nat. Photonics* **2012**, *6*, 605; c) K. Liu, C. R. Ye, S. Khan, V. J. Sorger, *Laser Photonics Rev.* **2015**, *9*, 172.

[3] P. Y. Yu, M. Cardona, in *Fundamentals of Semiconductors: Physics and Materials Properties* Springer, Berlin, Heidelberg **2010**, Ch. 1, pp. 1–15.

[4] a) E. Fortunato, P. Barquinha, R. Martins, *Adv. Mater.* **2012**, *24*, 2945; b) V. A. Vashchenko, V. F. Sinkevitch, in *Physical Limitations of Semiconductor Devices*, Springer-Verlag, Boston **2008**, Ch. 1, pp. 1–24.

[5] a) L. Zhang, Y. Zhou, L. Guo, W. Zhao, A. Barnes, H.-T. Zhang, C. Eaton, Y. Zheng, M. Brahlek, H. F. Haneef, N. J. Podraza, Moses H. W. Chan, V. Gopalan, K. M. Rabe, R. Engel-Herbert, *Nat. Mater.* **2016**, *15*, 204; b) D. S. Ginley, J. D. Perkins, in *Handbook of Transparent Conductors*, (Ed: D. S. Ginley), Springer, Boston, MA **2011**, Ch. 1, pp. 1–25; c) C. Zhang, C. Ji, Y.-B. Park, L. J. Guo, *Adv. Opt. Mater.* **2021**, *9*, 2001298.

[6] H. Hosono, K. Ueda, in *Springer Handbook of Electronic and Photonic Materials*, (Eds: S. Kasap, P. Capper), Springer International Publishing, Cham **2017**, Ch. 58, pp. 1391–1404.

[7] Y. Gui, M. Miscuglio, Z. Ma, M. H. Tahersima, S. Sun, R. Amin, H. Dalir, V. J. Sorger, *Sci. Rep.* **2019**, *9*, 11279.

[8] a) J. Paul, M. Miscuglio, Y. Gui, V. J. Sorger, J. K. Wahlstrand, *Opt. Lett.* **2021**, *46*, 428; b) M. Z. Alam, I. D. Leon, R. W. Boyd, *Science* **2016**, *352*, 795; c) D. Traviss, R. Bruck, B. Mills, M. Abb, O. L. Muskens, *Appl. Phys. Lett.* **2013**, *102*, 121112.

[9] J. Wu, Z. T. Xie, Y. Sha, H. Y. Fu, Q. Li, *Photon. Res.* **2021**, *9*, 1616.

[10] a) S. Shrestha, Y. Wang, A. C. Overvig, M. Lu, A. Stein, L. D. Negro, N. Yu, *ACS Photonics* **2018**, *5*, 3526; b) S. Bang, J. Kim, G. Yoon, T. Tanaka, J. Rho, *Micromachines* **2018**, *9*, 560; c) J. Zhao, C. Zhang, Q. Cheng, J. Yang, T. J. Cui, *Appl. Phys. Lett.* **2018**, *112*, 073504.

[11] K. Chen, P. Guo, T. D. Dao, S.-Q. Li, S. Ishii, T. Nagao, R. P. H. Chang, *Adv. Opt. Mater.* **2017**, *5*, 1700091.

[12] M. Miscuglio, Y. Gui, X. Ma, Z. Ma, S. Sun, T. El Ghazawi, T. Itoh, A. Alù, V. J. Sorger, *Commun. Phys.* **2021**, *4*, 196.

[13] R. Amin, R. Maiti, Y. Gui, C. Suer, M. Miscuglio, E. Heidari, R. T. Chen, H. Dalir, V. J. Sorger, *Optica* **2020**, *7*, 333.

[14] J.-J. Lin, Z.-Q. Li, *J. Phys. Condens. Matter* **2014**, *26*, 343201.

[15] a) P. D. C. King, T. D. Veal, *J. Phys. Condens. Matter* **2011**, *23*, 334214; b) R. G. Egdell, in *Defects at Oxide Surfaces*, (Eds: J. Jupille, G. Thornton), Springer International Publishing, Cham **2015**, Ch. 12, pp. 351–400.

[16] a) O. Bierwagen, *Semicond. Sci. Technol.* **2015**, *30*, 024001; b) X. Leng, A. T. Bollinger, I. Božović, *Sci. Rep.* **2016**, *6*, 31239; c) J. Nomoto, H. Matsui, I. Yamaguchi, T. Nakajima, T. Tsuchiya, *Appl. Phys. Lett.* **2021**, *118*, 101602; d) P. D. C. King, T. D. Veal, D. J. Payne, A. Bourlange, R. G. Egdell, C. F. McConville, *Phys. Rev. Lett.* **2008**, *101*, 116808.

[17] F. Werner, *J. Appl. Phys.* **2017**, *122*, 135306.

[18] M. Mazur, R. Pastuszek, D. Wojcieszak, D. Kaczmarek, J. Domaradzki, A. Obstarczyk, A. Lubanska, *Circuit World* **2020**, *48*, 149.

[19] Z. Q. Li, J. J. Lin, *J. Appl. Phys.* **2004**, *96*, 5918.

[20] C. S. S. Sangeeth, M. Jaiswal, R. Menon, *J. Appl. Phys.* **2009**, *105*, 063713.

[21] M. G. Sousa, A. F. da Cunha, *Appl. Surf. Sci.* **2019**, *484*, 257.

[22] a) T. Ohyama, M. Okamoto, E. Otsuka, *J. Phys. Soc. Jpn.* **1985**, *54*, 1041; b) Y.-J. Zhang, Z.-Q. Li, J.-J. Lin, *Phys. Rev. B* **2011**, *84*, 052202; c) J. W. Cleary, E. M. Smith, K. D. Leedy, G. Grzybowski, J. Guo, *Opt. Mater. Express* **2018**, *8*, 1231.

[23] a) T. Koida, *Phys. Status Solidi A* **2017**, *214*, 1600464; b) T. Koida, J. Nomoto, *Phys. Rev. Mater.* **2022**, *6*, 055401.

[24] J. Wróbel, G. A. Umana-Membreno, J. Boguski, D. Sztenkiel, P. P. Michałowski, P. Martyniuk, L. Faraone, J. Wróbel, A. Rogalski, *Phys. Status Solidi RRL* **2020**, *14*, 1900604.

[25] S. Złotnik, J. Wróbel, J. Boguski, M. Nyga, M. A. Kojdecki, J. Wróbel, *Sensors* **2021**, *21*, 5272.


© 2022 The Authors. physica status solidi (RRL) Rapid Research Letters published by Wiley-VCH GmbH

[26] G. A. Umana-Membreno, Y. Song, N. D. Akhavan, J. Antoszewski, D. C. Paine, A. Zaslavsky, L. Faraone, *Microelectron. Eng.* **2017**, *178*, 164.
[27] G. A. Umana-Membreno, J. Antoszewski, L. Faraone, *Microelectron. Eng.* **2013**, *109*, 232.
[28] a) H. Zhao, W. Li, Y. Chen, C. Xu, B. Li, W. Luo, D. Qian, Z. Shi, *Sci. Rep.* **2021**, *11*, 6249; b) J. Wang, A. Kurzendorfer, L. Chen, Z. Wang, Y. Ando, Y. Xu, I. Miotkowski, Y. P. Chen, D. Weiss, *Appl. Phys. Lett.* **2021**, *118*, 253107.
[29] a) P. D. C. King, T. D. Veal, P. H. Jefferson, S. A. Hatfield, L. F. J. Piper, C. F. McConville, F. Fuchs, J. Furthmüller, F. Bechstedt, H. Lu, W. J. Schaff, *Phys. Rev. B* **2008**, *77*, 045316; b) L. F. J. Piper, T. D. Veal, M. J. Lowe, C. F. McConville, *Phys. Rev. B* **2006**, *73*, 195321.
[30] D. C. Look, K. D. Leedy, M. D. Santia, S. C. Badescu, *Commun. Mater.* **2021**, *2*, 33.
[31] S. Dasgupta, M. Lukas, K. Dössel, R. Kruk, H. Hahn, *Phys. Rev. B* **2009**, *80*, 085425.
[32] a) Y. Kanai, *Jpn. J. Appl. Phys.* **1984**, *23*, L12; b) D. H. Zhang, H. L. Ma, *Appl. Phys. A* **1996**, *62*, 487; c) N. Kikuchi, E. Kusano, H. Nanto, A. Kinbara, H. Hideo, *Vacuum* **2000**, *59*, 492; d) J. W. Bae, S. D. Park, N. G. Cho, D. H. Lee, G. Y. Yeom, *Jpn. J. Appl. Phys.* **2002**, *41*, L999; e) K. Ellmer, R. Mientus, *Thin Solid Films* **2008**, *516*, 4620; f) A. Valla, P. Carroy, F. Ozanne, D. Muñoz, *Sol. Energy Mater. Sol. Cells* **2016**, *157*, 874; g) E. Sharika, M. Anjitha, K. Arya, N. Nair, S. Kiran, V. Vanagith, V. T. Babu, S. K. Ram, *Mater. Today Proc.* **2022**, *49*, 2131.


© 2022 The Authors. physica status solidi (RRL) Rapid Research Letters published by Wiley-VCH GmbH